

FIRBACK: III. Catalog, Source Counts, and Cosmological Implications of the $170\ \mu\text{m}$ ISO* Deep Survey

Hervé Dole^{1,2}, Richard Gispert¹, Guilaine Lagache¹, Jean-Loup Puget¹, François R. Bouchet³, Catherine Cesarsky⁴, Paolo Ciliegi⁵, David L. Clements⁶, Michel Dennefeld³, François-Xavier Désert⁷, David Elbaz^{8,9}, Alberto Franceschini¹⁰, Bruno Guiderdoni³, Martin Harwit¹¹, Dietrich Lemke¹², Alan F. M. Moorwood⁴, Sebastian Oliver^{13,14}, William T. Reach¹⁵, Michael Rowan-Robinson¹³, and Manfred Stickel¹²

¹ Institut d'Astrophysique Spatiale, bâtiment 121, Université Paris Sud, F-91405 Orsay Cedex, France

² *present address:* Steward Observatory, University of Arizona, 933 N Cherry Ave, Tucson, AZ 85721, USA

³ Institut d'Astrophysique de Paris, 98bis Bd Arago, F-75014 Paris, France

⁴ ESO, Karl-Schwarzschild-Strasse 2, D-85748 Garching bei München, Germany

⁵ Osservatorio Astronomico di Bologna, Via Ranzani 1, I-40127 Bologna, Italy

⁶ Department of Physics & Astronomy, Cardiff University, PO Box 813, Cardiff CF22 3YB, UK

⁷ Laboratoire d'Astrophysique, Obs. de Grenoble, B.P. 53, 414 av. de la piscine, F-38031 Grenoble cedex 9, France

⁸ Service d'Astrophysique, DAPNIA, DSM, CEA Saclay, F-91191, Gif-sur-Yvette, France

⁹ Physics and Astronomy Departments, University of California, Santa Cruz, CA 95064, USA

¹⁰ Astronomy Department, Padova University, Vicolo Osservatorio, 5, I-35122 Padova, Italy

¹¹ 511 H. Street S. W., Washington DC 20024-2725, USA; also Cornell University

¹² Max-Planck-Institut für Astronomie, Königstuhl 17, D-69117 Heidelberg, Germany

¹³ Astrophysics Group, Imperial College, Blackett Laboratory, Prince Consort Road, London SW7 2BZ, UK

¹⁴ Astronomy Centre, University of Sussex, Falmer, Brighton BN1 9QJ, UK

¹⁵ IPAC, California Institute of Technology, Pasadena, CA 91125, USA

Received 22-Jan-2001; accepted 9-March-2001.

Abstract. The FIRBACK (Far Infrared BACKground) survey is one of the deepest imaging surveys carried out at $170\ \mu\text{m}$ with ISOPHOT onboard ISO, and is aimed at the study of the structure of the Cosmic Far Infrared Background. This paper provides the analysis of resolved sources. After a validated process of data reduction and calibration, we perform intensive simulations to optimize the source extraction, measure the confusion noise ($\sigma_c = 45\ \text{mJy}$), and give the photometric and astrometric accuracies. 196 galaxies with flux $S > 3\sigma_c$ are detected in the area of 3.89 square degrees. Counts of sources with flux $S > 4\sigma_c$ present a steep slope of 3.3 ± 0.6 on a differential "logN-logS" plot between 180 and 500 mJy. As a consequence, the confusion level is high and will impact dramatically on future IR deep surveys. This strong evolution, compared with a slope of 2.5 from Euclidian geometry, is in line with models implying a strongly evolving Luminous Infrared Galaxy population. The resolved sources account for less than 10% of the Cosmic Infrared Background at $170\ \mu\text{m}$, which is expected to be resolved into sources in the 1 to 10 mJy range.

Key words. cosmology: miscellaneous – galaxies: infrared – galaxies: evolution – galaxies: statistics

1. Introduction

The European Space Agency's Infrared Space Telescope, ISO (Kessler et al., 1996; Kessler, 2000) performed about 1000 programs between 1995 and 1998, including the deepest extragalactic observations ever made in the mid- and

far-infrared range with an unprecedented sensitivity (for a review see Genzel & Cesarsky (2000)). Most of these deep cosmological observations aim at probing galaxy formation and evolution, mainly by resolving the Cosmic Infrared Background (CIB) into discrete sources, but also by studying the CIB fluctuations.

* Based on observations with ISO, an ESA project with instruments funded by ESA Member States (especially the PI countries: France, Germany, the Netherlands and the United Kingdom) and with the participation of ISAS and NASA.

Correspondence to: hdole@as.arizona.edu

Understanding and observing the sources contributing to the extragalactic background at all wavelengths has become one of the most rapidly evolving fields in observational cosmology since the discovery of the CIB (Désert et al., 1995; Puget et al., 1996). In particular, deep ob-

servations from space with ISO, and from the ground with SCUBA on the JCMT and MAMBO on the IRAM 30m telescope, respectively in the infrared, submillimeter and millimeter range, together with observations at other wavelengths for source identification (in the radio and optical / NIR range), begin to provide a global view of galaxy evolution. The long wavelength observations reveal galaxies through their dust emission, providing a complementary and significantly different view to that of optical and UV observations.

The ISO legacy regarding galaxy evolution includes a number of significant studies. About a dozen deep surveys have been conducted in the mid infrared with ISOCAM (Cesarsky et al., 1996), reaching sensitivity levels of $30\ \mu\text{Jy}$ at $15\ \mu\text{m}$ (Altieri et al., 1999; Elbaz et al., 1999; Aussel et al., 1999; Désert et al., 1999; Flores et al., 1999). The major results of the mid-infrared surveys involve source counts obtained by combining a number of surveys. These exhibit strong evolution with a steep slope up to 2.4 ± 0.2 (Elbaz et al., 1999) in the integral logN-logS diagram. Multiwavelength identifications and redshift distributions constrain the nature of the sources (Flores et al., 1999; Aussel et al., 1999; Chary and Elbaz, 2001): most of them are Luminous Infrared Galaxies, LIRG's, at a median redshift of 0.8.

In the far-infrared, the $60 - 240\ \mu\text{m}$ spectral domain was explored using the imaging capabilities of ISOPHOT (PHT) (Lemke et al., 1996). As indicated in Figure 1 of Gispert et al. (2000), this domain corresponds to the maximum emission of the extragalactic background. The main surveys published were carried out in the Lockman Hole on 1.1 sq. deg. at 90 and $170\ \mu\text{m}$ by Kawara et al. (1998), in the FIRBACK Marano field at $170\ \mu\text{m}$ by Puget et al. (1999) and in the entire FIRBACK survey by Dole et al. (1999), in SA57 on 0.4 sq. deg. at 60 and $90\ \mu\text{m}$ by Linden-Vornle et al. (2000), and in 8 small fields covering nearly 1.5 sq. deg. at 90, 120, 150 and $180\ \mu\text{m}$ by Juvella et al. (2000). A shallower survey was performed over an area of 11.6 sq. deg. at $90\ \mu\text{m}$ by Efstathiou et al. (2000) as part of the ELAIS survey. The ISOPHOT Serendipity Survey at $170\ \mu\text{m}$ (Stickel et al., 1998, 2000) took advantage of ISO slews between targets to detect about 1000 sources between 1 and 1000 Jy.

In the 60 to $120\ \mu\text{m}$ spectral windows, the C_100 camera, with its 3×3 array of Ge:Ga detectors, was subject to strong transients and spontaneous spiking, limiting the sensitivity (which is a few times better than IRAS); fortunately, new attempts to overcome these problems with a physical model of the detector seem promising (Coulais et al., 2000; Lari & Rodighiero, 2001). At 60 and $90\ \mu\text{m}$, no clear evolution in the source counts is observed, since both non-evolution and moderate evolution models can still fit the data (Linden-Vornle et al., 2000; Efstathiou et al., 2000). Furthermore, the K-correction¹ (Figure 1 from the

model of Dole (2000) and Lagache et al. (2001)) between 30 and $120\ \mu\text{m}$ is not favorable for probing galaxy evolution up to redshifts $z \sim 1$. With the ELAIS survey, Serjeant et al. (2001) were able to derive the luminosity function of galaxies up to redshift $z \simeq 0.3$.

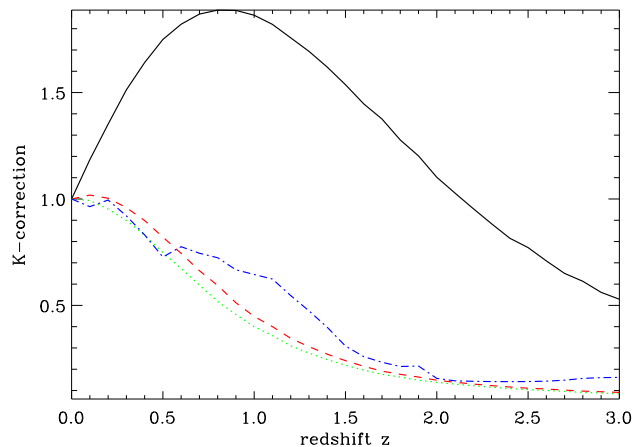


Fig. 1. K-corrections at 15 (dot-dashed curve), 60 (dotted curve), 90 (dashed curve) and $170\ \mu\text{m}$ (solid curve) for a LIRG (Dole, 2000; Lagache et al., 2001). The wavelengths of cosmological interest are thus around $15\ \mu\text{m}$ and above $150\ \mu\text{m}$ where they benefit from the “negative K-correction effect”, increasing the sensitivity up to redshifts around unity.

At longer wavelengths ($120-240\ \mu\text{m}$), the C_200 camera, a 2×2 array of stressed Ge:Ga detectors, is more stable and most of the detectors’ behaviour can be characterized and, if needed, properly corrected (Lagache & Dole, 2001). The K-correction at $170\ \mu\text{m}$ (Figure 1), as well as in the mid-infrared around $15\ \mu\text{m}$, is favorable and becomes optimal at redshifts around 0.7. The first analysis of deep surveys at $170\ \mu\text{m}$ showed a large excess in source counts over predictions of no-evolution models at flux levels below 200 mJy (Kawara et al., 1998; Puget et al., 1999), suggesting strong evolution. Recent work by Juvella et al. (2000) is in agreement with this picture, and includes the far-infrared colors of the sources.

The FIRBACK survey (acronym for Far Infrared BACKground) was designed to broaden our understanding of galaxy evolution with its accurate source counts and its catalog allowing multiwavelength follow-up. It also enabled studies of the CIB fluctuations (first detected in the first area surveyed in the FIRBACK program by Lagache & Puget (2000)). FIRBACK is one of the deepest surveys made at $170\ \mu\text{m}$ and the largest at this depth. This survey used about 150h of observing time, corresponding to the 8th largest ISO program (Kessler, 2000).

The aim of this paper is to provide the catalogs and the source counts of the FIRBACK survey. Preliminary FIRBACK source counts were published by Lagache et al.

¹ K-correction is defined as the ratio: $\frac{L(\nu')}{L(\nu)}$ where $L(\nu)$ is the luminosity at frequency ν , and $\nu = (1+z)\nu'$. Thus, $K(z) = \frac{L(\nu \times [1+z])}{L(\nu)}$.

(1998) and Puget et al. (1999) on the 0.25 sq. deg. Marano 1 field, and by Dole et al. (2000) on the entire survey. An overview of this paper is as follows. Section 2 presents the observational issues of the FIRBACK survey and Section 3 summarizes the data processing and the calibration (a complete description can be found in Lagache & Dole (2001)). Section 4 explains the extensive simulations and the source extraction technique. Section 5 details the flux measurement by aperture photometry, analyses the photometric and astrometric noise of the sources and provides estimates of accuracies. In section 6 we present the final FIRBACK catalog ($S > 4\sigma_s$), and the complementary catalog ($3\sigma_s < S < 4\sigma_s$) extracted for follow-up purposes. Section 7 describes the corrections that have been applied (completeness, Malmquist-Eddington effect) and presents the final FIRBACK source counts at 170 μm . Section 8 compares our results to other observations as well as models, and discusses the cosmological implications of the FIRBACK source counts: strong evolution and resolution of the CIB.

2. The FIRBACK survey: Fields & Observations

2.1. Fields

FIRBACK is a survey at 170 μm covering four square degrees in three high galactic latitude fields, called FIRBACK South Marano (FSM), FIRBACK North 1 (FN1) and FIRBACK / ELAIS North 2 (FN2) (see Table 1). They were chosen to have foreground contaminations as low as possible: the typical HI column-density is less than or equal to $N_H \simeq 10^{20} \text{cm}^{-2}$, and the 100 μm brightness is less than 1.7 MJy/sr on DIRBE maps. In addition, FN1 and FN2 were chosen to match some fields from the European Large Area ISO Survey, ELAIS (Oliver et al., 2000), which had been covered at 15 μm with ISOCAM (Serjeant et al., 2000) and at 90 μm with ISOPHOT (Efstathiou et al., 2000). FN2 observation time is a collaboration between the ELAIS and FIRBACK consortia.

Table 1. *Fields of the FIRBACK survey at 170 μm*

field	α_{2000}	δ_{2000}	l	b	S_{100}^a
FSM	03 ^h 11 ^m	-54° 45'	270°	-52°	1.42
FN1	16 ^h 11 ^m	+54° 25'	84°	+45°	1.17
FN2	16 ^h 36 ^m	+41° 05'	65°	+42°	1.19

^a Mean brightness at 100 μm (MJy/sr) in DIRBE maps (annual average, zodiacal component subtracted)

2.2. Observations

Observations were carried with ISO, using the ISOPHOT spectro-photo-polarimeter. We used the C_200 2 \times 2 pixel photometer and C_160 broadband filter centered at $\lambda = 170 \mu\text{m}$. Scanning the sky was done in raster map mode,

Table 2. *Observational characteristics of the FIRBACK fields*

field	FSM1	FN1	FN2
area (sq. deg.)	0.95	1.98	0.96
rasters ^b	4	2	2
redundancy ^c	16	8	8
t_{int}^d (sec)	256	128	128
raster step ^e (pixels)	1,1, 2,2 ^a	1,1	1,1
offset ^f (pixels)	0.5,0.5 1,1 ^a	< 1 ^g	< 1 ^g
date	Nov-1997 Jul-1997 ^a	Dec-1997	Jan-1998
revolution ^h	739 to 744 593 ^a	753 to 774	785 to 798

^a in the case of the FSM1 field only

^b number of different rasters mapping the same field

^c number of different observations per sky pixel on the center of final coadded map

^d integration time per sky pixel on the center of final coadded map

^e offset in pixel in the Y and Z directions of the spacecraft between the steps on the raster

^f offset in pixel between different rasters

^g offset is irregular due to the rotation of the fields

^h ISO revolution numbers (or number range) of observation

AOT P22, with one pixel offset between each pointing, to provide the redundancy. Individual rasters were shifted with respect to each other by a fraction of a pixel to provide proper sampling where possible. Table 2 summarizes the observational characteristics of the fields.

The FSM field is composed, for historical reasons, of four individual fields, called FSM1, 2, 3 and 4 (Figure 6 in Lagache & Dole (2001)). FSM1 on the one hand, and FSM2, 3 and 4 on the other, have been observed continuously: transient effects are thus reduced and no rotation of the field occurs between different rasters (same roll angle). FSM1 rasters are offset by two pixels in order to maximise redundancy and establish the ISOPHOT sensitivity for such observations, whereas FSM2, 3 and 4 are offset by a half pixel in both Y and Z directions to increase oversampling.

The FN1 field is composed of eleven individual fields (Figure 7 in Lagache & Dole (2001)), observed twice. Observations were not performed continuously, so that each individual raster has a different roll angle, giving a sampling of the sky that is non uniform.

The FN2 field is composed of nine individual fields (Figure 8 in Lagache & Dole (2001)), observed twice. The other characteristics are the same as for FN1.

3. Data Reduction, Instrumental Effects, Calibration, Maps

The complete process of data reduction and calibration is described in Lagache & Dole (2001). Here, we merely summarize the different steps.

3.1. Interactive Analysis

We made use of the PHT Interactive Analysis package (PIA) version 7.2.2 (Gabriel et al., 1997) in the IDL version 5.1 environment, to process the raw data (named ERD: Edited Raw Data) into brightnesses (named AAP: Astronomical and Application product). After linearizing and deglitching the ramps, we applied the orbit-dependent dark and reset interval corrections. We calibrated the data with the two bracketing FCS lamps (Fine Calibration Source) values, using the mean value in order not to induce baseline effects.

3.2. Glitches, Long Term Transients, Flat Fielding

Cosmic particles hitting the detector are easy to detect at the time of their impact, but they may cause response variations. On 224 different measurements (that is 56 independent rasters observed by 4 pixels), we report only 13 such cases, which are corrected. Furthermore, thanks to the high redundancy of each raster, a glitch cannot mimic a source because the same piece of the sky is observed independently by the four pixels of the photometer at different times.

Some long term transients (LTT) are seen in the data, and are understood to be the consequence of step fluxes seen by the photometer. During the FIRBACK observations, ISOPHOT was looking at relatively flat fields with low background, but was on more complex fields during the preceding observations. Our best data occur where the observations were made continuously. We correct for the LTT by forcing all the pixels to follow the time variations of the most stable pixel, which is assumed to represent the sky. This correction is found to be linear, and never exceeds 10 %.

We then compute a flat field using the redundancy and apply the necessary corrections. The detector behaviour is highly reproducible, leading to constant flat field values: 1.04 ± 0.02 , 0.91 ± 0.02 , 1.09 ± 0.02 and 0.94 ± 0.02 for pixels 1, 2, 3 and 4 respectively.

3.3. Photometric Correction

There is a difference of 11% between the solid angle value of the PHT footprint at $170\ \mu\text{m}$ used by PIA and the value derived by calibration observations around Saturn and the model. We thus apply a multiplicative correcting factor of 0.89 to the brightness values given by PIA to take into account the real profile of the footprint.

3.4. Maps

For a given raster measurement, we project the signal from each pixel on a regular grid defined by the raster. Between each pointing, we make an interpolation and check that the photometry is not changed by more than 1%. Then we sum all these signals on a celestial coordinate grid to get the final map.

3.5. Calibration of Extended Emission

Using the knowledge of the average interstellar dust emission spectrum, the zodiacal light emission at the time of the observations, and the Cosmic Infrared Background values derived from COBE, together with HI data on our fields, we derive a brightness value at $170\ \mu\text{m}$ for each of our fields. This extrapolated brightness at $170\ \mu\text{m}$ for the three fields is in remarkable agreement with the measured ISOPHOT brightness. Furthermore, the rejection level of straylight up to 60° off-axis observed by ISO during total solar eclipse by the Earth, is better than 10^{-13} , implying that there is no significant contribution to the measured flux coming from the far sidelobes. This confirms that ISO is able to make absolute measurements of the extended emission and gives a high degree of confidence to our photometric calibration.

4. Source Extraction, Simulations

An important part of the present work is the extraction of the sources, the simulation of point source observations and the analyses of noise. After detecting sources on a median-filtered-like map, we measure the fluxes on the final maps with aperture photometry. Our simulation tool validates the flux determination as well as the noise analysis.

4.1. Source Extraction

Our original maps are dominated by the fluctuations of the background at $170\ \mu\text{m}$, at all spatial scales, mainly due to the cirrus confusion noise and the CIB fluctuations (Lagache & Puget, 2000). Because of this, classical extraction algorithms based on thresholding and local background determination mostly fail: it is not easy to use a robust detection algorithm on maps dominated by structures at all scales. On the contrary, flat background maps allow reliable detection with the available processing techniques, like gaussian fitting methods, e.g. for faint ISOCAM sources by Désert et al. (1999). Because of the undersampling of the PHT Point Spread Function together with a highly fluctuating background, CLEAN-like methods (Hogbom, 1974) are difficult to use. Wavelet decomposition, e.g. for ISOCAM by Starck et al. (1999), is not easily implementable because of the poor spatial dynamics of our maps (“big pixels and small maps”). To overcome these difficulties we have developed the follow-

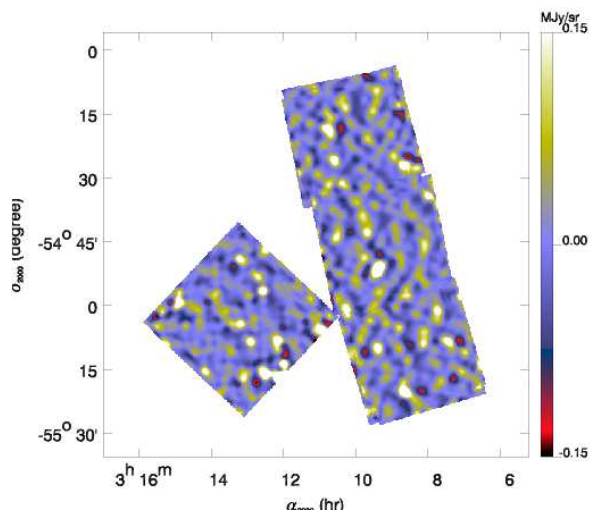


Fig. 2. Example of a *source map* for source detection in the FSM field. Background is subtracted using a median filter in the time space (AAP). Data with only high spatial frequencies are then reprojected on a map with the FIRBACK pipeline.

ing method by combining some well-known techniques for source extraction and flux determination:

- background is subtracted in the one dimensional time data (AAP level, brightness as a function of time) using a median filter (size: 5 positions) to create *source time data*
- *source time data* are processed to create 2-dimensional *source maps* (Figure 2) through the FIRBACK pipeline as described in Section 3
- source detection is performed on the *source maps* using SExtractor (Bertin & Arnouts, 1996)
- flux measurements are performed on the unfiltered maps, using aperture photometry at the positions found by the source detection only if there are at least 4 different observations, and make a temporary version of the source catalog
- by subtracting iteratively the brightest sources from the temporary catalog using a CLEAN-like method on the final maps, we remeasure with better accuracy the flux of the sources which have bright neighbours. This gives the final catalog after two more corrections: short term transient of 10%, and flux offset of about 15% derived from simulation (see Section 5).

Source detection is performed using SExtractor version 2.1.0 on the *source maps* with the parameters given in Table 3. Note that we do not use the background estimator and set it to a constant value because *source maps* are flat maps containing fluctuations due to resolved sources, since the background has been filtered. Only the positions in the map of the detected sources will be used in the output catalog computed by SExtractor (e.g. not the flux). We discard the edges by considering only parts of the sky that

Table 3. Parameters used in SExtractor 2.1.0 applied on the *Source Maps*

Parameter	Value
DETECT_MINAREA	10
DETECT_THRESH	3.0
BACK_SIZE	10
BACK_FILTERSIZE	1,1
BACK_TYPE	MANUAL
BACK_VALUE	-0.04,0.0

have been observed at least 4 times. This reduces the total area by about 5%.

4.2. Simulations

We have developed a simulation tool of point sources in order to validate the flux determinations and study source completeness of our survey. Kawara et al. (1998) did not make such simulations and Juvela et al. (2000) only tested the significance of their source detection because of a lack of redundancy in their observations. The work of Efstathiou et al. (2000) included large simulations at $90\ \mu\text{m}$, but the source detection is performed by eye.

Thanks to the quiet behaviour of the C200 camera at $170\ \mu\text{m}$, together with redundancy, the detector noise as well as effects induced by glitches can be neglected to first order with respect to the confusion noise. (This is unlike conditions applying to the C100 camera (Linden-Vornle et al., 2000).)

Here, we present a summary of our simulation process, followed by some details concerning the addition of the sources and the validation:

- select a random sky position for a simulated source inside a FIRBACK field
- add the source in each raster in AAP level which has observed the source itself or its wings
- process maps through the FIRBACK pipeline
- extract sources with SExtractor
- identify the extracted sources by comparing the coordinates with the input catalog
- compute a flux with aperture photometry using the effective footprint (defined in Section 5.1)
- validate on different flat backgrounds
- validate on real data: different input fluxes and positions

4.2.1. Adding the Sources

We use the best footprint available for PHT at $170\ \mu\text{m}$ (Lagache & Dole, 2001) to simulate a source with a known input flux; its spatial extension is taken to be a five pixel square, that is about $7.7' \times 7.7'$ (note that the PIA footprint profile given in the calibration files extends to only

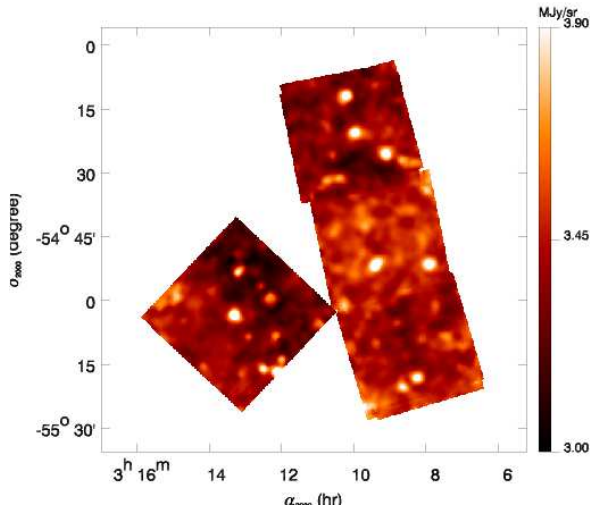


Fig. 3. Example of the addition of 500 mJy sources in the FSM field. There are 8 sources spread randomly throughout the field. One example is near the center of the eastern survey square (FSM1).

4.2 arcminutes). This simulated source is added in the one dimensional time data (AAP level). To avoid biases due to specific positions in the fields, we select random positions.

Because we have either 2 or 4 different raster observations of the same parts of the sky, the randomly-selected sky position may fall e.g. on the edge of a pixel in one raster, and at the center of another pixel in another raster. We thus make the following approximation: we cut each PHT pixel in 9 square sub-pixels of about 30.7×30.7 square arcseconds. We compute the pixelized footprint for the nine configurations corresponding to the cases where the source center falls on one of the sub-pixels.

We make separate realizations for 8 input fluxes (100, 150, 200, 300, 500, 650, 800 and 1000 mJy) and create maps using the FIRBACK pipeline. We add only between 6 and 20 sources per square degree at a time depending on their flux, in order to avoid changing the confusion level when sources are added in the data. We compute the needed number of maps to get 1200 realizations for each flux in each field, or 28800 sources in total, in order to have a statistically significant sample. We finally get about 2×1230 different simulated maps per field (1 final map + 1 source map for each realization) taking about 14 Gbyte, after about one week of computation under IDL on a MIPS R12000 at 300MHz SGI. Fig. 3 shows an example of added sources.

4.2.2. Validation

We extract sources on the final maps and compute fluxes as explained below by aperture photometry. The aperture photometry filter parameters have been optimized to obtain the best signal to noise ratio using the simulations.

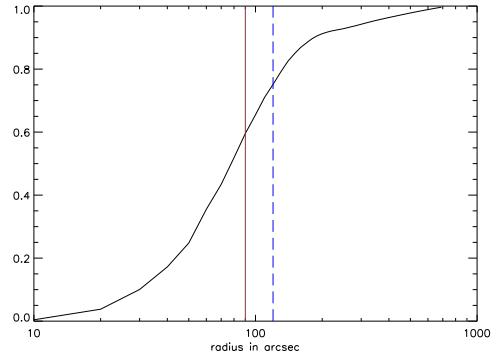


Fig. 4. Growth curve of the effective footprint on a logarithmic scale with the location of the radii of circles used for aperture photometry; dotted vertical line: 90 arcsecond for the inner radius; dashed vertical line: 120 arcsecond for the outer radius.

The validation is performed on flat background maps with different surface brightness values (0.01, 3 and 10 MJy/sr), to check that the recovered flux does not depend on the background. The difference between the input and recovered flux is less than 1% on an individual raster when the source is centered on a pixel. When using random positions of the sources and 2 or 4 rasters co-added, the recovered fluxes have a dispersion explained by the “edge effect” (due to the dilution of the flux in other pixels when the source falls on the edge of a pixel) and by the poor sampling of the sky, leading to an overall uncertainty of 10%.

5. Photometry, Noise Analysis, Accuracy

5.1. Flux Measurements by Aperture Photometry

Once a detection is obtained on source maps, fluxes have to be measured in final maps. Simulations of point sources on a flat background permit derivation of the *effective average footprint* on the map, which results from the PHT footprint and the final pixeling obtained in a given field, which depends on the exact timing of the observations (roll angle).

We check that strong sources in the data have a profile in agreement with the effective footprint. The growth curve of the effective footprint is plotted in Fig. 4. The determination of the parameters for the aperture photometry filter is performed by measurements of the flux of simulated sources through different sets of apertures.

We find that the following values minimize the noise: an internal radius of 90 arcseconds for measuring the source and an external radius of 120 arcseconds to estimate the background. The determination of the flux takes into account the fact that at these radii we select only a part of the effective footprint, and includes the appropriate correction.

In order not to be biased by a nearby strong source which could affect the estimate of the local background in

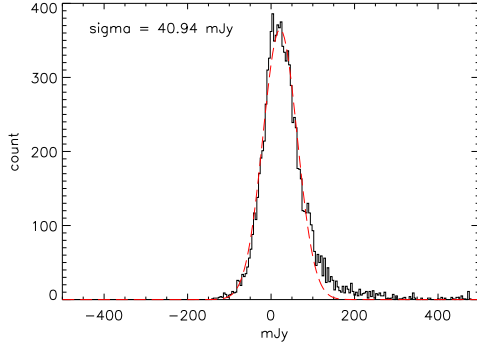


Fig. 5. 10000 random aperture photometry measurements on the FSM map indicating the confusion noise. The small excess at high flux levels is due to real sources in the data.

a measurement, we used a CLEAN-like procedure. We first compute a temporary catalog that we sort by decreasing flux. Then we measure the brightest source, and remove it, and repeat this process through the whole catalog. Note that this procedure is not used to extract faint sources but only to improve the photometry of sources detected before applying the CLEAN procedure.

At the end of the process, we add 10% to the source flux to account for the transient behaviour of the detector. This value is derived from our absolute measurement in the FSM1 (using AOT P25) in which the instantaneous response and the following transient, as well as the final flux after 256 seconds, are observed (Lagache & Dole, 2001).

5.2. Confusion Noise

We made 10000 measurements on each field at random positions, and obtained distributions which are shown on figures 5, 6 and 7. These distributions represent the probability of measurements by aperture photometry on a field with sources and dominated by confusion. They are fitted in their central part by a gaussian, whose dispersion is an estimate of the confusion noise. The distributions are plotted in Fig. 5 to 7. The asymmetric part at high flux levels reflects the counts of bright sources. We finally derive $\sigma_c \simeq 45$ mJy for the confusion noise in all of the FIRBACK fields (41 mJy for FSM, 44 for FN1 and 46 mJy for FN2). The $3\sigma_c$ level is thus 135 mJy and $4\sigma_c$ 180 mJy.

This estimate is compatible with the classical definition of the confusion, by computing the number of independent beams in all the FIRBACK fields: with a FWHM of 94 arcseconds at $170\ \mu\text{m}$ in a 3.89 sq. deg. surface, we have about 5700 independent beams. At the 3σ limit, that is above 135 mJy, we have 196 sources (see Sect. 6), there are about 29 beams per source — in good agreement with the classical definition of the confusion of 30 independent beams per source for sources brighter than $3\sigma_c$. If we have a catalogue cutoff at $4\sigma_c$ (resp. $5\sigma_c$), we obtain 54 (resp 91) independent beams per source. Our analysis is compati-

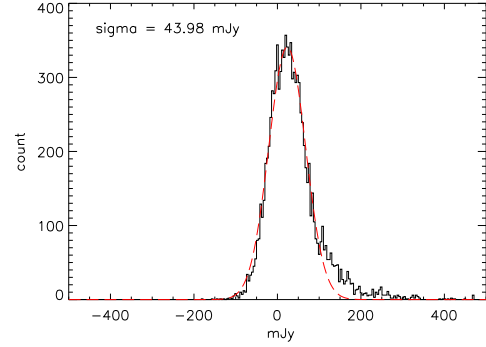


Fig. 6. 10000 random aperture photometry measurements on FN1.

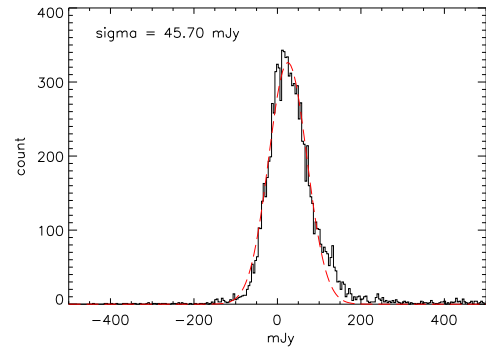


Fig. 7. 10000 random aperture photometry measurements on FN2.

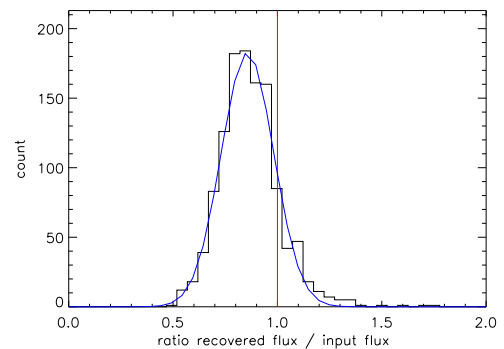


Fig. 8. Histogram of the ratio of measured flux to input flux, when sources of 500 mJy are added to the maps.

ble with the simulations of Hogg (2000), who shows that 30 beams per source is a minimum where source counts are steep, and suggests a threshold at about 50 beams per source.

The cirrus fluctuations have a low probability of creating spurious sources at this level of HI column-density, as shown in previous works, such as Gautier et al. (1992), Lagache (1998), Kawara et al. (1998), Puget et al. (1999), and Juvela et al. (2000).

5.3. Detector Noise

The first field to be observed in our investigations was FSM1, and the goal was to demonstrate the ability of doing a deep far infrared survey limited by confusion rather than detector noise. With four independent rasters mapping exactly the same sky, that is 16 independent measurements, Lagache (1998) and Puget et al. (1999) show that the detector noise level is about 3 mJy 1σ , i.e. far below the confusion noise and thus neglected.

5.4. Photometric Accuracy

The histograms of the ratio of recovered flux to input flux of the simulated sources are used to estimate the offset and the error of the fluxes. One of these histograms is shown in figure 8 for the FN1 field and 500 mJy sources.

One can see a systematic offset of the distribution's peak with respect to the input flux. This offset is constant for a given field, and equals 16%, 19%, 18% and 16% for the FN1, FN2, FSM1 and FSM234 fields, respectively. The possible explanations for this offset are (1) the variation of the effective footprint inside the field (due to an inhomogeneous sampling of the sky) and (2) the loss of flux at the edges of the pixels. We apply this correction on the source fluxes.

The standard deviation of the fitted gaussian, σ_s , estimates the dispersion of the source flux measurements. Figure 10 shows the variation of σ_s in mJy as a function of the source flux in Jy, in the FN1 field; the variation is similar in the other fields. σ_s can be decomposed in two components:

- a constant component due to confusion noise σ_c
- a component (σ_p) proportional to the source flux, due to the difference between the mean effective footprint and the local effective footprint.

The data points are fitted by the quadratic sum of the constant and the proportional component $\sqrt{\sigma_c^2 + \sigma_p^2}$.

The source flux uncertainties are computed for each field; however, there is little field-to-field variation. The uncertainty in the source flux is about 25% near $3\sigma_c$ at low fluxes, about 20% near $5\sigma_c$ and decreases to about 10% at high flux levels (near 1 Jy).

5.5. Positional Accuracy

The identification of the sources in the simulations allows us to derive the positional accuracy. We neglect the telescope absolute pointing error of 1" (Kessler, 2000). Fig. 11 shows the distribution of the distance offset between the input source and the extracted source positions. All sources brighter than 500 mJy — i.e. where the sample is complete (see Sect. 7.1) — are recovered inside a 65" radius: the mean recovered distance is 15", and 90% of the sample falls inside 28". Taking all the sources with flux levels brighter than 180 mJy, 90% of the sample is

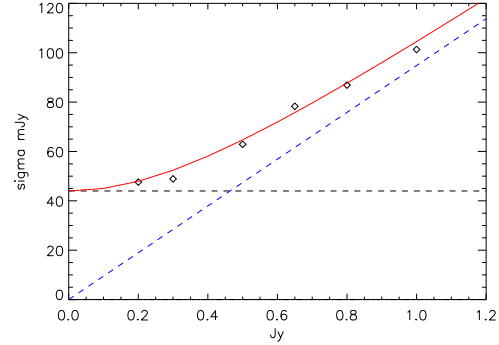


Fig. 10. Evolution of σ_s , standard deviation of measured flux on the histograms, as a function of the source flux (diamonds). σ_s can be decomposed in two components: (1) a constant component due to confusion noise σ_c (horizontal dashed line) and (2) a component proportional to the flux σ_p (sloped dashed line). σ_s is fitted by $\sqrt{\sigma_c^2 + \sigma_p^2}$ (solid line).

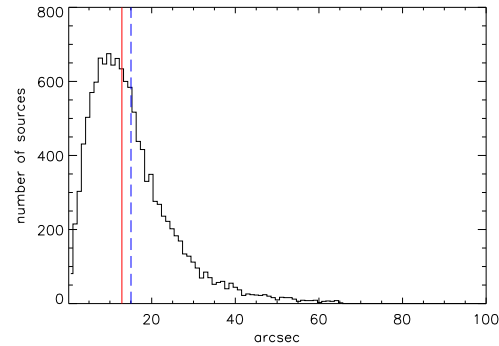


Fig. 11. Histogram of distances of identifications in the simulations. All sources brighter than 500 mJy (where the sample is complete) in the three FIRBACK fields are shown. The solid line corresponds to the median at 13 arcseconds and the dashed line at 15 arcseconds.

recovered inside a radius of 42". We conclude that 99% (respectively 93%) of the sources are found in a circle of radius of 50", and 98% (respectively 90%) in 42" when the sample is complete, above 500 mJy (respectively 180 mJy).

6. FIRBACK Source Catalogs

6.1. ISO FIRBACK Source Catalog

The final catalog, the *ISO FIRBACK Source Catalog* (IFSC), contains 106 sources with fluxes between 180 mJy (4σ) and 2.4 Jy. The catalog is given for each field in tables 7 to 10. All the sources have been checked for detection in all individual measurements. It is interesting to note that above $5\sigma_c$ the source density is constant in the fields, with 16 sources in FSM, 15 in FN2, and 32 sources in

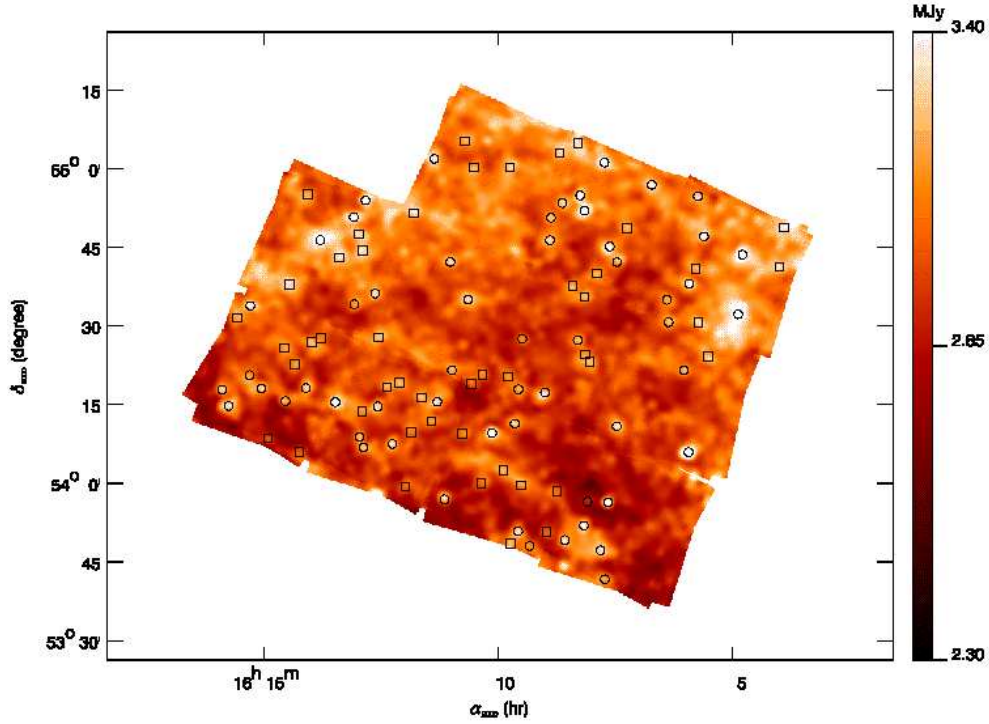


Fig. 9. Detected sources on FN1 field. Circles are sources from the ISO FIRBACK Source Catalog ($S_\nu > 180$ mJy) and squares are sources from the Complementary ISO FIRBACK Source Catalog ($135 < S_\nu < 180$ mJy).

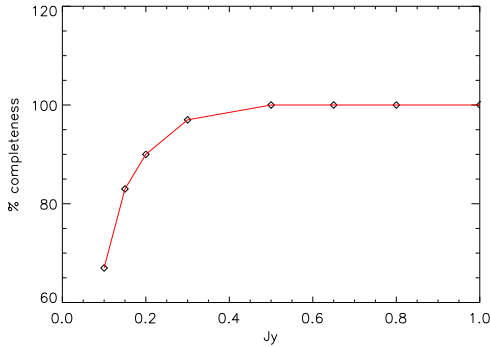


Fig. 12. Completeness of the FIRBACK catalog, computed from the simulations as the ratio of the number of detected sources to the number of added sources.

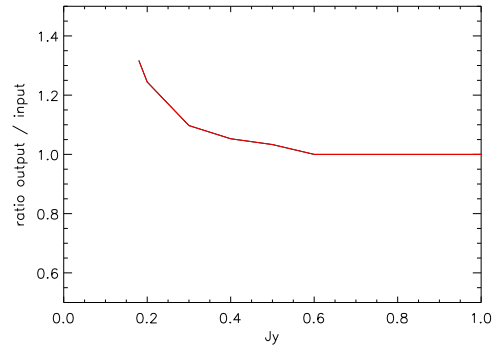


Fig. 13. Malmquist-Eddington bias. Ratio of simulated source counts to simulated observed source counts. Due to flux uncertainties, the number of counts is overestimated at low flux levels.

FN1 which is twice the size of the other fields. The source density is thus 16 ± 4 sources brighter than 225 mJy per square degree. At the $4\sigma_c$ limit, the source density is 27 ± 5 sources brighter than 180 mJy per square degree, with a larger field-to-field dispersion. The brightest sources in FSM lie at 497 and 443 mJy, in FN1 at 838, 597 and 545 mJy, and in FN2 at 2377, 1251, 803, 682, 666 and 522 mJy.

6.2. Complementary ISO FIRBACK Source Catalog

Sources with flux levels above the $3\sigma_c$ limit are higher redshift candidates and they can be used for statistical study of the nature of $170\ \mu\text{m}$ sources. Nevertheless, the lower signal to confusion-noise ratio leads to lower flux accuracy — reduced to about 25% at 135 mJy — and may include spurious sources: this larger uncertainty suggests avoiding the use of these sources, e.g. in the counts.

Candidates for $z > 1$ may be selected on the basis of photometric redshift using the FIR-radio correlation

(Condon, 1992; Helou et al., 1985) and the submillimetre-radio correlation (Carilli & Yun, 2000). The success of recent submillimetre detections of FIRBACK sources with SCUBA at the JCMT (Scott et al., 2000, with an rms sensitivity of 2 mJy,) and with MAMBO at IRAM-30m (with an rms sensitivity better than 0.5 mJy, Lagache et al., in prep) in the millimetre range confirms the relevance of this technique.

Table 4. Number of sources per flux bin in $3.89^{\circ 2}$ used for the source counts, without any correction.

flux min (mJy)	flux max (mJy)	number per bin	cumulative number
180.0	190.0	13	106
190.0	210.0	20	93
210.0	240.0	21	73
240.0	300.0	24	52
300.0	500.0	19	28
500.0	∞	9	9

In this frame of mind, we compile a Complementary ISO FIRBACK Source Catalog (CIFSC, tables 11 to 13 for each field) which contains 90 sources whose flux levels lie in the range 135 to 180 mJy (3 to $4\sigma_c$). All the sources have been checked for detection in all individual measurements. There are 15 sources in FSM, 47 in FN1, and 28 in FN2. As an example, Fig 9 shows of the detected sources in the FN1 field. At this flux level, the source density is not constant between the fields and fluctuates at about 23 ± 8 sources per square degree in the range 135 - 180 mJy.

7. Source Counts

7.1. Completeness

Simulations allow us to derive the completeness, that is the ratio at a given flux between the number of added sources and the number of detected ones. The completeness is plotted in Fig. 12. Our sample is complete above 500 mJy, and is about 90% (respectively about 85%) complete above 225 mJy (respectively 180 mJy). We thus correct the surface source density for this incompleteness.

7.2. Malmquist-Eddington Bias

Uncertainties in the flux determination introduce an excess in the number of counts, known as the Malmquist-Eddington bias. We characterize it with the results of the simulations, by comparing the effect of a flux dispersion on a known input source count model: a simple power law. Fig. 13 shows the ratio of an input source count model, to the simulated observations of this model. We apply the appropriate correction to the data: at 225 mJy (respectively 180 mJy) the raw counts have to be decreased by

20% (respectively 30%). We check that these values are not more sensitive than 5% (respectively 10%) at $5\sigma_c$ (respectively $4\sigma_c$) to the power law of the input model in the range 3.0 - 3.6.

7.3. FIRBACK Source Counts

Figure 14 shows the differential source counts at 170 μm coming from the FIRBACK survey (3.89 sq. deg.), with 106 sources between 180 (4σ) and 2400 mJy. The horizontal error bar gives the flux uncertainty, and the vertical error bar the poisson noise in \sqrt{n} where n is the number of sources in the bin.

The statistics of sources used for source counts before any correction is given in Table 4. The integral (respectively differential) source count values are given in Table 5 (respectively Table 6). Note that for the differential counts we took only 5 sources in the last flux box, corresponding to highest fluxes (between 500 and 700 mJy).

The two points at high flux levels are compatible with no evolution since we can adjust a horizontal line inside the error bars. The slope of the differential source counts is not constant, but can reasonably be fitted by a linear of slope 3.3 ± 0.6 between 180 and 500 mJy.

Table 5. FIRBACK Integrated Source Counts.

\log_{10} of galaxy density (sr^{-1})	flux (mJy)
4.919 ± 0.085	180.0 ± 21.5
4.869 ± 0.090	190.0 ± 21.8
4.774 ± 0.102	210.0 ± 22.6
4.638 ± 0.121	240.0 ± 23.6
4.374 ± 0.166	300.0 ± 25.8
3.894 ± 0.301	500.0 ± 33.0

8. Discussion

8.1. Comparison with other Work

Kawara et al. (1998) estimated the confusion level to be 45 mJy, and extracted 45 sources brighter than 150 mJy ($3\sigma_c$) in the 1.1 sq. deg. Lockman Hole field. Juvela et al. (2000) found $\sigma_c = 44$ mJy, and detected 55 sources brighter than 150 mJy in 1.5 sq. deg. Both these estimates are consistent with our measurements.

Our raw results are in agreement with the pioneering work on $1/16^{\text{th}}$ of the area of the entire FIRBACK survey by Lagache (1998) and Puget et al. (1999). Without completeness or Malmquist-Eddington bias correction, our catalogs are similar. Of the 24 sources of Puget et al. (1999), we detect 18. The six missing sources are: (1) on the edges of the field with fewer observations than required

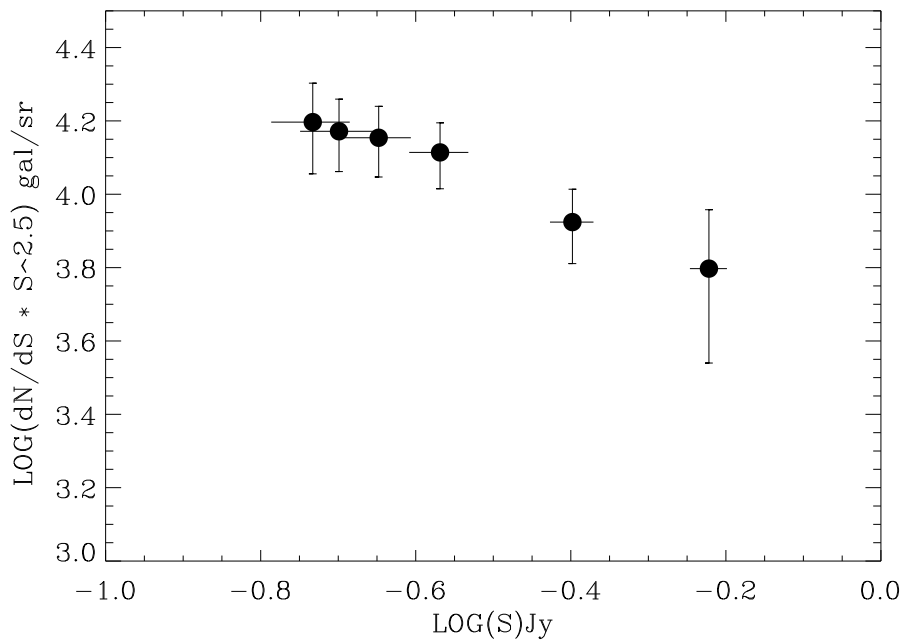


Fig. 14. FIRBACK differential source counts (normalized to Euclidian counts) at 170 μm . 106 sources are brighter than 180 mJy ($4\sigma_c$) on 3.89 sq. deg. The slope of the differential source counts is 3.3 ± 0.6 between 180 and 500 mJy.

in our procedure of extraction for three of their sources, and (2) in more confused regions for the other three.

For the 18 common sources, the photometry is in excellent agreement (except for one source which is near the edge of the field). Both analyses find 13 sources at fluxes higher than 150 mJy in this field.

In our preliminary work (Dole et al., 1999, 2000), we detected the sources by eye and used the same photometry as Puget et al. (1999) for consistency, but we did not remove bright sources to measure the fainter sources. Statistically, these efforts are compatible with our current source counts.

8.2. Comparison with Models

Table 6. FIRBACK Differential Source Counts.

\log_{10} of $\frac{dN}{dS} \times S^{2.5}$ ($\text{sr}^{-1} \times \text{Jy}^{1.5}$)	flux bin (mJy)
4.179 ± 0.247	180 – 190
4.157 ± 0.198	190 – 210
4.143 ± 0.193	210 – 240
4.107 ± 0.180	240 – 300
3.921 ± 0.203	300 – 500
3.797 ± 0.418	500 – 700

The semi-analytical model from Guiderdoni et al. (1998) was used in the FIRBACK proposal to justify the integration time and surface coverage, and has been improved recently (Devriendt & Guiderdoni, 2000). Our phenomenological model (Dole et al., 2000) was developed by taking into account all the observational constraints in the infrared and submillimetre range, and is based on strong evolution of a bright population of galaxies. Both models are presented in Fig. 15. The models of Franceschini et al. (1998), with and without evolution, are shown in Fig. 16 together with the pure luminosity evolution model of Rowan-Robinson (2001).

The data unambiguously reject models without evolution or with low evolution at flux levels fainter than 500 mJy. The no-evolution model of Franceschini et al. (1998) (dots in Fig. 16) and the model without ULIRGs (Sanders & Mirabel, 1996) of Guiderdoni et al. (1998) (dotted line in Fig. 15) are incompatible with the data: they predict between 5 and 10 times fewer sources than observed.

Model E of Guiderdoni et al. (1998) with strong evolution and an addition of ULIRGs underestimates the source counts by a factor of 2, and predicts a lower slope than the observations. Nevertheless, the agreement within a factor of 2 between model E and the final observed source counts is quite remarkable: this model was developed to account for the CIB, and was used for predicting the FIRBACK source counts at the time of submission of this observing program. The phenomenological model of Dole et al. (2000) fits the data at faint fluxes, as well as the model of Rowan-Robinson (2001).

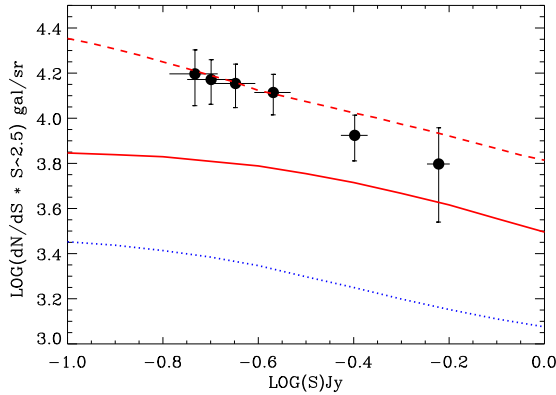


Fig. 15. FIRBACK differential source counts at $170\ \mu\text{m}$ with models from Guiderdoni et al. (1998) with evolution and without ULIRG's (A, dotted line) and with evolution with ULIRG's (E, solid line), and from Dole et al. (2000) (strongly evolving LIRGs, dashed line).

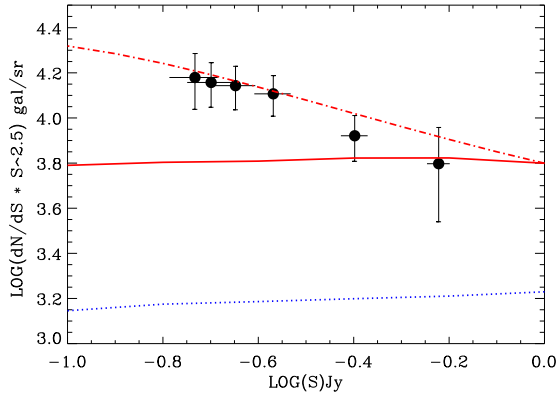


Fig. 16. FIRBACK differential source counts at $170\ \mu\text{m}$ with models from Franceschini et al. (1998) without evolution (dotted line) and with evolution (solid line), and from Rowan-Robinson (2001) (pure luminosity evolution, dot-dashed line).

Other semi-analytical models like e.g. Blain et al. (1999), or phenomenological models like e.g. those of Tan et al. (1999), Xu et al. (2000), and Pearson (2000), also try to reproduce the spectrum of the CIB as well as the source counts in the whole spectral domain from the mid infrared (sometimes optical) to the sub-millimeter (sometimes centimeter) range. It is beyond the scope of this paper to compare all these models with our observations, but scenarios without strong evolving populations of LIRGs are uniformly unable to reproduce the data.

8.3. Resolving the Cosmic Infrared Background at $170\ \mu\text{m}$

We now ask what fraction of the CIB is contributed by sources brighter than $135\ \text{mJy}$ at $170\ \mu\text{m}$? Since the flux integral is dominated by sources at lower flux levels, it is rather simple to compute its value on the assumption that source counts have a constant slope. We estimate that $4 \pm 1\%$ of the CIB is resolved into sources brighter than $135\ \text{mJy}$.

Using the model of Dole et al. (2000), we show that 7% of the CIB is resolved in sources brighter than $135\ \text{mJy}$.

Thus, the population of individually observed sources in the FIRBACK survey does not dominate the CIB at this wavelength.

We can also ask at which flux levels the CIB will be largely resolved at $170\ \mu\text{m}$? The observed slope of the source counts may be extrapolated to lower flux levels to predict a convergence. The expected flattening of the source counts close to the convergence is neglected, and thus the derived values give an upper limit. With this proviso, we find that the $170\ \mu\text{m}$ background should be resolved at flux levels in the range 10 to $20\ \text{mJy}$, an order of magnitude fainter than the ISO sensitivity.

Using our model presented in Fig. 15, we predict that 80 to 90% of the CIB should be resolved in the range 2 to $5\ \text{mJy}$.

The required sensitivity at $170\ \mu\text{m}$, about 60 times better than ISO, is not reachable with the 1m-class space infrared observatories such as NASA's SIRTF. SIRTF should be able to break about 15-30% of the background into discrete sources at $160\ \mu\text{m}$. 4m-class ESA's Herschel (former FIRST) should be able to break the bulk of the background.

8.4. Survey Optimisation and Confusion

While the confusion is found to be identical in the 3 FIRBACK fields at about $45\ \text{mJy}$ (regardless of sampling), the FSM fields have been observed twice as frequently as the northern fields. This means that the confusion limit was reached faster than expected. Two years after the end of the observations, and five years after the launch of ISO, our analysis shows that the best (ideal) observational strategy would have been to repeat the individual observations (rasters) 4 times to obtain enough redundancy (done in the FSM field) with less integration and proper over-sampling. With this optimisation, we could have gained 25% more surface with the earned time, or performed complementary observations at another wavelength.

An early proper determination of the confusion level is thus a key factor for extragalactic infrared surveys from space, since the confusion is high due to the strong evolution, and limits the surveys. It is challenging, given the relatively short time spend in the "Performance Verification" or "In Orbit Checkout" phases that normally precede routine astronomical observations in space.

9. Conclusion & Summary

The analysis of the FIRBACK ISO deep survey sources at 170 μm is presented. After a process of data reduction and calibration of extended emission (Lagache & Dole, 2001), we performed extensive simulations to validate our source extraction process, and studied the sources of noise and accuracy in photometry and astrometry. The confusion σ_c equals 45 mJy.

We compiled the ISO FIRBACK Source Catalog ($S_{170} > 4\sigma_c$) and the Complementary ISO FIRBACK Source Catalog ($3\sigma_c < S_{170} < 4\sigma_c$, for follow-up purposes) containing 196 sources. It is important to note that the extended source calibration is in excellent agreement with DIRBE and the point source calibration is in agreement with IRAS. The differential source counts show a steep slope of 3.3 ± 0.6 between 180 and 500 mJy, and a significant excess of faint sources with respect to low or moderate evolution expectations.

The steep slope of the source counts has important consequences on the sensitivity limits of the deep surveys conducted in the far infrared: the confusion noise is large, as it will be for future observatories, and will impact dramatically on the future IR deep surveys.

One important intention of the FIRBACK survey was to probe the nature of the extragalactic far-infrared sources. According to most of the models, the steep slope of the source counts is due to a strongly evolving population of LIRGs. Our model shows that the effect of the K-correction alone is insufficient to explain the observations. To definitively investigate this question, one has to identify the sources and understand their nature. Discussions of the nature of the FIRBACK sources is beyond of the scope of this paper and will be discussed elsewhere. The multiwavelength follow-up performed at 1.4 GHz, 1.3 mm, 850 & 450 μm , as well as other ISO and optical / NIR data, seems to show that most of the sources (typically 50%) are local ($z < 0.3$), and about 10% at high redshift ($z > 1$). Massive star formation seems also to be dominant. Nevertheless, identifying FIRBACK sources is not easy because of the uncertainty in the positions at 170 μm .

The summary of the FIRBACK survey is as follows:

- observation of about 4 sq. deg. in 3 high galactic latitude fields: FSM, FN1 & FN2
- ISOPHOT AOT P22 raster map mode with the C_200 array and the C_160 filter at 170 μm
- 128 or 256 seconds of integration per sky pixel
- extraction of instrumental effects: long and short term transients, photometric correction
- calibration of extended emission: excellent agreement between PHT and DIRBE
- calibration of point sources compatible with IRAS
- instrumental noise: 3 mJy 1σ
- confusion noise: 45 mJy 1σ ; $4\sigma_c$ sensitivity: 180 mJy
- ISO FIRBACK Source Catalog: 106 sources between 180 mJy and 2.4 Jy
- Complementary ISO FIRBACK Source Catalog: 90 sources between 135 and 180 mJy
- Flux uncertainty error: 25% at $3\sigma_c$, 20% at $5\sigma_c$, and reduced to 10% at higher flux levels
- positional error: 100 arcsecond diameter circle (99% of the sources)
- source density for $S_{170} > 225$ mJy: 16 ± 4 sources per square degree
- source density for $S_{170} > 180$ mJy: 27 ± 5 sources per square degree
- slope of the differential source counts: 3.3 ± 0.6 between 180 and 500 mJy
- 4 to 7% of the Cosmic Infrared Background at 170 μm is resolved into sources brighter than 135 mJy
- Prediction that the CIB will be resolved at flux levels in the range 1 to 10 mJy at 170 μm
- Catalogs, images, and plots available on line at: <http://wwwfirback.ias.u-psud.fr>

Acknowledgements. HD, GL & JLP appreciate discussions with Rene Laureijs and Carlos Gabriel at Vilspa and Ulrich Klaas at Heidelberg. We also are grateful to Alain Abergel, Alain Coulais & Marc-Antoine Miville-Deschênes at IAS, for stimulating and helpful discussions through the analysis of the FIRBACK data. Thanks also go to Martin Kessler and his team who did a great job in planning ISO observations so efficiently. MH acknowledges support of his participation on ISO through NASA grants and contracts. DE acknowledges support from NASA grant NAG5-8218.

References

- Altieri, B, Metcalfe, L, Kneib, J. P. et al. 1999, *A&A*, 343:L65.
- Aussel, H, Cesarsky, C. J, Elbaz, D, & Starck, J. L. 1999, *A&A*, 342:313.
- Bertin, E & Arnouts, S. 1996, *A&As*, 117:393.
- Blain, A. W, Jameson, A, Smail, I, et al. 1999, *MNRAS*, 309:715.
- Carilli, C. L & Yun, M. S. 2000, *ApJ*, 530:618.
- Cesarsky, C. J, Abergel, A, Agnese, et al. 1996, *A&A*, 315:L32.
- Chary, R, and Elbaz, D. 2001, *ApJ*, in press, astro-ph/0103067
- Condon, J. J. 1992, *ARA&A*, 30:575.
- Coulais, A, Fouks, B. I, Giovannelli, et al. In *SPIE 2000*, 2000.
- Désert, F. X, Abergel, A, Bernard, J. P, et al. In Dwek, E, editor, *Unveiling the Cosmic Infrared Background*, page 96. AIP Conference Proceedings 348, 1995.
- Désert, F. X, Puget, J. L, Clements, D. L, et al. 1999, *A&A*, 342:363.
- Devriendt, J. E. G & Guiderdoni, B. 2000, *A&A*, 363:851.
- Dole, H, Lagache, G, Puget, et al. In Cox, P & Kessler, M, editors, *The Universe as Seen by ISO, Paris, Unesco, 1998, astro-ph/9902122*, page 1031. ESA-SP/427, 1999.
- Dole, H, Gispert, R, Lagache, et al. In Lemke, Stickel, Wilke, Eds *ISO view of a Dusty Universe, Ringberg*,

Table 7. FIRBACK Catalog in FSM: coordinates are in hours (α_{2000}) or degrees (δ_{2000}), minutes, seconds, the flux S and the flux uncertainty δS at 170 μm are in mJy.

source	α_{2000}	δ_{2000}	S	δS	S/σ_c
FSM_000	3 09 25	-54 52 04	497	52	11.0
FSM_001	3 12 07	-55 17 09	443	50	9.9
FSM_002	3 12 29	-55 16 30	420	49	9.3
FSM_003	3 11 59	-55 14 20	369	46	8.2
FSM_004	3 08 37	-55 20 45	365	46	8.1
FSM_005	3 10 22	-54 31 55	301	43	6.7
FSM_006	3 10 45	-54 32 05	300	43	6.7
FSM_007	3 12 10	-55 09 00	296	43	6.6
FSM_008	3 12 33	-54 57 00	269	42	6.0
FSM_009	3 08 42	-54 27 28	267	41	5.9
FSM_010	3 10 16	-55 01 37	261	41	5.8
FSM_011	3 12 53	-55 09 28	239	40	5.3
FSM_012	3 08 03	-54 34 33	232	40	5.2
FSM_013	3 15 18	-55 01 26	228	40	5.1
FSM_014	3 14 50	-54 59 09	226	40	5.0
FSM_015	3 10 37	-54 26 16	225	40	5.0
FSM_016	3 13 07	-54 49 40	214	39	4.8
FSM_017	3 08 24	-54 28 04	210	39	4.7
FSM_018	3 10 01	-55 11 45	207	39	4.6
FSM_019	3 07 28	-55 09 07	202	39	4.5
FSM_020	3 09 31	-55 25 04	200	38	4.4
FSM_021	3 08 50	-55 05 45	190	38	4.2
FSM_022	3 09 24	-55 10 37	182	38	4.1

Table 8. FIRBACK Catalog in FN1: coordinates are in hours (α_{2000}) or degrees (δ_{2000}), minutes, seconds, the flux S and the flux uncertainty δS at 170 μm are in mJy.

source	α_{2000}	δ_{2000}	S	δS	S/σ_c
FN1_000	16 05 52	54 06 46	838	90	18.6
FN1_001	16 07 37	53 57 25	597	73	13.3
FN1_002	16 10 07	54 10 40	545	69	12.1
FN1_003	16 12 55	54 54 57	408	59	9.1
FN1_004	16 11 09	53 58 01	391	58	8.7
FN1_005	16 04 44	54 32 56	374	57	8.3
FN1_006	16 04 37	54 44 16	348	55	7.7
FN1_007	16 13 32	54 16 22	338	54	7.5
FN1_008	16 08 58	54 18 25	335	54	7.4
FN1_009	16 08 05	54 53 02	313	52	7.0
FN1_010	16 09 34	53 51 57	309	52	6.9
FN1_011	16 08 09	53 52 58	304	52	6.8
FN1_012	16 12 17	54 08 31	302	51	6.7
FN1_013	16 07 38	55 02 13	300	51	6.7
FN1_014	16 15 51	54 15 18	295	51	6.6
FN1_015	16 07 25	54 11 52	294	51	6.5
FN1_016	16 07 32	54 46 12	289	51	6.4
FN1_017	16 05 48	54 38 56	288	50	6.4
FN1_018	16 14 11	54 19 01	288	50	6.4
FN1_019	16 12 36	54 15 39	285	50	6.3
FN1_020	16 08 11	54 55 58	283	50	6.3
FN1_021	16 13 11	54 51 43	271	49	6.0
FN1_022	16 16 00	54 18 25	270	49	6.0
FN1_023	16 08 33	53 50 16	270	49	6.0
FN1_024	16 09 38	54 12 28	266	49	5.9
FN1_025	16 08 35	54 54 32	243	47	5.4
FN1_026	16 14 37	54 16 26	241	47	5.3
FN1_027	16 11 25	55 02 59	234	47	5.2
FN1_028	16 07 42	53 42 43	229	46	5.1
FN1_029	16 11 19	54 16 37	229	46	5.1
FN1_030	16 05 28	54 47 52	228	46	5.1
FN1_031	16 11 03	54 43 19	225	46	5.0
FN1_032	16 12 41	54 37 11	224	46	5.0
FN1_033	16 13 00	54 09 50	224	46	5.0
FN1_034	16 07 23	54 43 12	221	46	4.9
FN1_035	16 15 25	54 34 30	218	45	4.8
FN1_036	16 06 36	54 57 54	214	45	4.7
FN1_037	16 15 09	54 18 46	210	45	4.7
FN1_038	16 07 48	53 48 14	207	45	4.6
FN1_039	16 08 50	54 51 46	205	45	4.6
FN1_040	16 09 28	54 28 40	205	45	4.5
FN1_041	16 08 15	54 28 22	204	44	4.5
FN1_042	16 10 39	54 36 10	202	44	4.5
FN1_043	16 05 57	54 22 26	201	44	4.5
FN1_044	16 09 33	54 19 01	198	44	4.4
FN1_045	16 08 51	54 47 27	198	44	4.4
FN1_046	16 12 55	54 07 48	196	44	4.4
FN1_047	16 08 04	53 57 32	196	44	4.4
FN1_048	16 11 00	54 22 40	192	44	4.3
FN1_049	16 13 09	54 35 05	186	43	4.1

Nov 1999, *astro-ph/0002283*. Springer Lecture Notes, 2000.

Dole, H. PhD thesis, Université Paris-Sud XI, Orsay, 2000.

Efstathiou, A, Oliver, S, Rowan-Robinson, M, et al. 2000, *MNRAS*, 319:1169.

Elbaz, D, Cesarsky, C. J, Fadda, D, et al. 1999, *A&A*, 351:L37.

Flores, H, Hammer, F, Désert, F. X, et al. 1999, *A&A*, 343:389.

Franceschini, A, Andreani, P, & Danese, L. 1998, *MNRAS*, 296:709.

Gabriel, C, Acosta-Pulido, J, Heinrichsen, I, et al. In Hunt, G & H. E. Payne, e, editors, *Astronomical Data Analysis Software and Systems VI*, page 108, 1997.

Gautier, T. N. I, Boulanger, F, Perault, M, & Puget, J. L. 1992, *AJ*, 103:1313.

Genzel, R & Cesarsky, C. J. 2000, *ARA&A*, 38:761.

Gispert, R, Lagache, G, & Puget, J. L. 2000, *A&A*, 360:1.

Guiderdoni, B, Hivon, E, Bouchet, F. R, & Maffei, B. 1998, *MNRAS*, 295:877.

Helou, G, Soifer, B. T, & Rowan-Robinson, M. 1985, *ApJ*, 298:L7.

Hogbom, J. A. 1974, *A&As*, 15:417.

Hogg, D. W. 2001, *AJ*, 121:1207.

Juvela, M, Mattila, K, & Lemke, D. 2000, *A&A*, 360:813.

Kawara, K, Sato, Y, Matsuhara, H, et al. 1998, *A&A*, 336:L9.

Kessler, M. F, Steinz, J. A, Anderegg, M. E, et al. 1996, *A&A*, 315:L27.

Table 9. FIRBACK Catalog in FN1 (continued).

source	α_{2000}	δ_{2000}	S	δS	S/σ_c
FN1_050	16 13 55	54 47 16	185	43	4.1
FN1_051	16 05 35	54 55 37	185	43	4.1
FN1_052	16 06 16	54 31 37	183	43	4.1
FN1_053	16 09 19	53 49 08	182	43	4.0
FN1_054	16 15 25	54 21 17	182	43	4.0
FN1_055	16 06 18	54 35 52	180	43	4.0

Table 10. FIRBACK Catalog in FN2: coordinates are in hours (α_{2000}) or degrees (δ_{2000}), minutes, seconds, the flux S and the flux uncertainty δS at 170 μm are in mJy.

source	α_{2000}	δ_{2000}	S	δS	S/σ_c
FN2_000	16 37 33	40 52 26	2377	213	52.8
FN2_001	16 35 08	40 59 20	1251	139	27.8
FN2_002	16 36 10	41 05 16	803	102	17.8
FN2_003	16 35 25	40 55 51	682	92	15.2
FN2_004	16 34 01	41 20 49	666	91	14.8
FN2_005	16 32 43	41 08 38	522	78	11.6
FN2_006	16 35 06	41 10 51	346	62	7.7
FN2_007	16 35 45	40 39 14	316	60	7.0
FN2_008	16 35 47	41 28 58	293	58	6.5
FN2_009	16 33 55	40 53 13	291	57	6.5
FN2_010	16 35 38	41 16 58	285	57	6.3
FN2_011	16 38 07	40 58 12	260	55	5.8
FN2_012	16 34 13	40 56 45	249	54	5.5
FN2_013	16 34 08	40 50 52	244	53	5.4
FN2_014	16 38 24	41 13 19	235	52	5.2
FN2_015	16 36 07	40 55 37	223	51	5.0
FN2_016	16 34 26	40 54 07	218	51	4.9
FN2_017	16 34 44	41 08 42	213	50	4.7
FN2_018	16 33 38	41 01 15	212	50	4.7
FN2_019	16 37 17	40 48 36	205	49	4.6
FN2_020	16 32 41	41 06 10	201	49	4.5
FN2_021	16 37 58	40 51 21	196	49	4.4
FN2_022	16 37 08	41 28 26	190	48	4.2
FN2_023	16 33 51	40 49 44	188	48	4.2
FN2_024	16 38 56	41 02 13	185	48	4.1
FN2_025	16 36 31	40 47 38	184	48	4.1
FN2_026	16 36 16	40 48 28	182	47	4.0

Kessler, M. F. In Casoli, F, Lequeux, J, & David, F, editors, *Infrared Space Astronomy, Today and Tomorrow*, page 29. Les Houches School, 1998, session LXX, 2000.

Lagache, G, Dole, H. & Puget, J. L. 2001, *A&A*, in prep.

Lagache, G & Dole, H. 2001, *A&A*, in press.

Lagache, G & Puget, J. L. 2000, *A&A*, 355:17.

Lagache, G, Abergel, A, Boulanger, F, & Puget, J. L. 1998, *A&A*, 333:L709.

Lagache, G. PhD thesis, Université Paris XI Orsay, 1998.

Lari, C. & Rodighiero, G. 2001, in prep.

Lemke, D, Klaas, U, Abolins, J, et al. 1996, *A&A*, 315:L64.

Table 11. FIRBACK Complementary Catalog in FSM: coordinates are in hours (α_{2000}) or degrees (δ_{2000}), minutes, seconds, the flux S and the flux uncertainty δS at 170 μm are in mJy.

source	α_{2000}	δ_{2000}	S	δS	S/σ_c
CFSM_023	3 14 06	-55 16 12	173	37	3.8
CFSM_024	3 07 48	-55 01 44	165	37	3.7
CFSM_025	3 13 15	-55 04 44	160	37	3.6
CFSM_026	3 09 43	-54 43 08	160	37	3.5
CFSM_027	3 13 05	-55 17 02	158	37	3.5
CFSM_028	3 09 28	-54 09 57	157	37	3.5
CFSM_029	3 08 38	-54 57 35	157	37	3.5
CFSM_030	3 10 46	-54 19 11	151	36	3.4
CFSM_031	3 13 50	-54 58 15	151	36	3.3
CFSM_032	3 09 41	-54 21 07	149	36	3.3
CFSM_033	3 12 41	-54 53 38	147	36	3.3
CFSM_034	3 10 31	-54 43 51	145	36	3.2
CFSM_035	3 08 09	-55 09 07	142	36	3.2
CFSM_036	3 11 36	-54 56 13	141	36	3.1
CFSM_037	3 08 54	-55 00 46	136	36	3.0

Linden-Vornle, M. J. D, Norgaard-Nielsen, H. U, Jorgensen, H. E, et al. 2000, *A&A*, 359:L51.

Oliver, S, Rowan-Robinson, M, Alexander, D. M, et al. 2000, *MNRAS*, 316:749.

Pearson, C. astro-ph/0011335, 2000.

Puget, J. L, Abergel, A, Bernard, J. P, et al. 1996, *A&A*, 308:L5.

Puget, J. L, Lagache, G, Clements, et al. 1999, *A&A*, 345:29.

Rowan-Robinson, M. 2001, *ApJ*, in press, astro-ph/0012022.

Sanders, D. B & Mirabel, I. F. 1996, *ARA&A*, 34:749.

Scott, D, Lagache, G, Borys, C, et al. 2000, *A&A*, 357:L5.

Serjeant, S, Oliver, S, Rowan-Robinson, M, et al. 2000, *MNRAS*, 316:768.

Serjeant, S, Efstathiou A, Oliver, S, et al. 2001, *MNRAS*, 322:262.

Starck, J. L, Aussel, H, Elbaz, D, et al. 1999, *A&As*, 138:365.

Stickel, M, Bogun, S, Lemke, et al. 1998, *A&A*, 336:116.

Stickel, M, Lemke, D, Klaas, U, et al. 2000, *A&A*, 359:865.

Tan, J. C, Silk, J, & Balland, C. 1999, *ApJ*, 522:579.

Xu, C, Lonsdale, C. J, Shupe, D. L, O'Linger, J, & Masci, F. astro-ph/0009220, 2000.

Table 12. FIRBACK Complementary Catalog in FN1: coordinates are in hours (α_{2000}) or degrees (δ_{2000}), minutes, seconds, the flux S and the flux uncertainty δS at 170 μm are in mJy.

source	α_{2000}	δ_{2000}	S	δS	S/σ_c
CFN1_056	16 11 40	54 17 24	179	43	4.0
CFN1_057	16 08 06	54 36 36	176	43	3.9
CFN1_058	16 14 18	54 06 46	175	42	3.9
CFN1_059	16 08 00	54 24 17	175	42	3.9
CFN1_060	16 11 26	54 12 54	168	42	3.7
CFN1_061	16 07 49	54 41 02	168	42	3.7
CFN1_062	16 14 25	54 23 27	168	42	3.7
CFN1_063	16 12 09	54 20 13	166	42	3.7
CFN1_064	16 08 21	54 38 42	166	42	3.7
CFN1_065	16 14 04	54 27 46	166	42	3.7
CFN1_066	16 11 51	54 52 37	165	42	3.7
CFN1_067	16 09 44	55 01 22	165	42	3.7
CFN1_068	16 10 46	54 10 37	165	42	3.7
CFN1_069	16 08 57	53 51 54	165	42	3.7
CFN1_070	16 15 42	54 32 09	164	42	3.7
CFN1_071	16 09 29	54 00 43	163	42	3.6
CFN1_072	16 13 03	54 48 32	161	41	3.6
CFN1_073	16 05 37	54 31 33	161	41	3.6
CFN1_074	16 08 43	53 59 38	161	41	3.6
CFN1_075	16 05 25	54 24 57	159	41	3.5
CFN1_076	16 09 53	54 03 36	159	41	3.5
CFN1_077	16 07 09	54 49 40	159	41	3.5
CFN1_078	16 12 37	54 28 51	158	41	3.5
CFN1_079	16 13 29	54 43 55	157	41	3.5
CFN1_080	16 10 32	55 01 22	154	41	3.4
CFN1_081	16 12 24	54 19 22	153	41	3.4
CFN1_082	16 05 39	54 41 45	151	41	3.4
CFN1_083	16 10 20	54 21 50	150	41	3.3
CFN1_084	16 14 12	54 55 58	149	41	3.3
CFN1_085	16 12 58	54 45 21	149	41	3.3
CFN1_086	16 10 22	54 01 08	148	40	3.3
CFN1_087	16 09 44	53 49 37	147	40	3.3
CFN1_088	16 14 34	54 38 38	146	40	3.3
CFN1_089	16 12 00	54 00 21	144	40	3.2
CFN1_090	16 14 59	54 09 17	143	40	3.2
CFN1_091	16 10 44	55 06 21	141	40	3.1
CFN1_092	16 10 34	54 20 02	140	40	3.1
CFN1_093	16 08 06	54 25 37	140	40	3.1
CFN1_094	16 13 52	54 28 33	138	40	3.1
CFN1_095	16 08 13	55 05 59	138	40	3.1
CFN1_096	16 03 49	54 41 49	138	40	3.1
CFN1_097	16 08 38	55 04 04	137	40	3.1
CFN1_098	16 11 53	54 10 44	137	40	3.0
CFN1_099	16 12 57	54 14 38	137	40	3.0
CFN1_100	16 03 42	54 49 15	136	40	3.0
CFN1_101	16 09 46	54 21 28	136	40	3.0
CFN1_102	16 14 40	54 26 34	135	40	3.0

Table 13. FIRBACK Complementary Catalog in FN2: coordinates are in hours (α_{2000}) or degrees (δ_{2000}), minutes, seconds, the flux S and the flux uncertainty δS at 170 μm are in mJy.

source	α_{2000}	δ_{2000}	S	δS	S/σ_c
CFN2_027	16 37 06	41 24 10	179	47	4.0
CFN2_028	16 36 35	40 56 06	178	47	4.0
CFN2_029	16 34 20	41 06 54	178	47	4.0
CFN2_030	16 35 23	40 38 42	178	47	4.0
CFN2_031	16 34 21	41 10 19	171	46	3.8
CFN2_032	16 35 03	41 31 37	168	46	3.7
CFN2_033	16 34 00	41 11 20	168	46	3.7
CFN2_034	16 34 12	40 46 26	166	46	3.7
CFN2_035	16 38 50	41 05 27	166	46	3.7
CFN2_036	16 37 01	40 43 08	165	46	3.7
CFN2_037	16 38 15	40 54 25	162	45	3.6
CFN2_038	16 34 32	41 22 37	161	45	3.6
CFN2_039	16 36 13	40 42 25	160	45	3.6
CFN2_040	16 36 45	41 31 22	158	45	3.5
CFN2_041	16 34 31	41 00 14	156	45	3.5
CFN2_042	16 35 59	40 37 33	155	45	3.4
CFN2_043	16 35 44	40 49 26	154	45	3.4
CFN2_044	16 37 26	40 45 39	150	44	3.3
CFN2_045	16 34 23	41 20 02	150	44	3.3
CFN2_046	16 36 04	40 30 21	147	44	3.3
CFN2_047	16 34 51	41 20 27	147	44	3.3
CFN2_048	16 37 37	40 57 00	145	44	3.2
CFN2_049	16 37 42	41 19 11	143	44	3.2
CFN2_050	16 37 18	41 16 04	142	44	3.2
CFN2_051	16 36 18	41 15 21	142	44	3.2
CFN2_052	16 34 06	41 03 10	141	44	3.1
CFN2_053	16 36 23	41 23 13	138	43	3.1
CFN2_054	16 36 56	41 14 09	136	43	3.0